

Application of Waveform Modeling to Determine Focal Mechanisms of the 1993 Tapu Earthquake and Its Aftershocks

TZAY-CHYN SHIN¹

(Manuscript received 4 December 1993, in final form 18 March 1994)

ABSTRACT

To determine the focal mechanisms of the 1993 Tapu earthquake sequence by applying the multiple station moment tensor inversion is the main objective of this paper. Digital strong motion seismograms recorded at short distance are used. The realistic layered model obtained by Ho and Shin (1994) is slightly modified to calculate the Green's functions and then the synthetic waveforms for moment tensor inversion.

Both fault plane solutions decomposed from moment tensor and the depth cross-section of aftershocks show that there were two earthquake sequences from 15, December 1993 to 30 January 1994. The first earthquake sequence was mainly formed by the Tapu main earthquake (ML=5.7). The focal depths were distributed between 10.0 and 17.0 km. The ruptural process was characterized by a westward dipping thrust fault. The second earthquake sequence occurred after 3, January 1994 and was located 20 km north of the first. The mainshock (ML=4.4) and aftershocks of the second sequence were located shallowly between 3.0 and 8.0 km. The fault plane solutions show a vertical normal faulting of southern dipping with a left-lateral component.

(Key words: 1993 Tapu earthquake, Moment tensor inversion)

1. INTRODUCTION

The Chia-Nan Plain in southwestern Taiwan has been ranked as an area with a high potential for large earthquakes because of the absence of a damaging earthquake in the past 29 years (Shin and Leu, 1986). In the recent years, the earthquake monitoring system in this area has been significantly improved. The digital seismograms recorded from earthquakes occurring in this area may provide important observations in understanding of the ruptural mechanism as well as local stress variation corresponding to local geological structure and tectonic features. In 1991, the Chiali earthquake (ML=5.67) was located to the west of the

¹ Central Weather Bureau, Kung Yuan Road 64, Taipei, Taiwan, R.O.C.

Chia-Nan seismic zone which was not a seismically active place before the occurrence of mainshock (Shin *et al.*, 1994). Although the earthquake caused only minor damage along the coastal area, it is believed not to be directly associated with the historical damaging earthquake zone in the Chia-Nan plain.

An earthquake of moderate magnitude 5.7 named as the Tapu earthquake occurred on 15, December 1993 and is the largest earthquake to have occurred in this area since 1964. The Taiwan Seismic Network (TaiSeiN) gave the location of the mainshock as 23.21°N , 120.52°E and the depth as 13.5 km which is very close to the last damaging earthquake (1964, Paiho earthquake; 23.2°N , 120.6°E) of $\text{ML}=6.5$. The mainshock was strongly felt in the Chia-Nan area where the largest peak ground motion acceleration (PGA) of 472 gal was recorded by station CHY018 which is 13.5 km away from the epicenter. The closest station (CHY019), at 5.9 km away, recorded a PGA value of 407 gal. Following the mainshock, there were more than 162 aftershocks among which 23 aftershocks had magnitudes greater than 3.0 and at least 8 were felt events according to the Central Weather Bureau (CWB) intensity scale.

CWB executing the Taiwan Strong Motion Instrument Program (TSMIP) has deployed a digital strong motion array around Taiwan. Many high dynamic range (16 bits A/D converter) and free field accelerographs have been installed in the Chia-Nan plain. The digital accelerograms recorded during the Tapu earthquake sequence have provided a good opportunity for a detailed investigation into the ruptural process of the earthquake and its aftershocks, especially considering the situation that all velocity seismograms of near stations are clipped. The object of this paper is to determine focal mechanisms of this earthquake sequence by the application of the moment tensor inversion technique. Both of P- and S-waves are used for waveform matching. Efforts are also made to correlate the focal mechanisms with the spatial distribution of aftershocks as well as the variation of local stress.

2. REGIONAL GEOLOGICAL SETTING AND SEISMICITY

The mainshock of the 1993 Tapu earthquake sequence occurred in Chia-Nan plain near to the Chukou active fault (Hsu and Chang, 1979). Figure 1 shows the seismicity in the central region of the Chia-Nan plain (120.3°E - 120.5°E ; 23.1°N - 23.5°N) during the time period of 1991 to June 1994. The thin line in this map indicates the boundary of the western coastal plains and the western foothills from the geological view of point (Ho, 1988). On the left is the geologic province of Quaternary alluvium consisting of clay, sand and gravel. The western foothill is the site of a late Cenozoic sedimentary basin which began in the Oligocene and continued into the early Pleistocene, which has been greatly folded and faulted. The long toothed solid line in Figure 1 is known as the Chukou fault and is one of the major thrust faults in southern Taiwan (Hsu and Chang, 1979). This fault strikes NNE for a distance of about 65 km. The sawteeth show the upthrust side of the fault. The short solid line in between is a NNE thrust fault known as the Muchuliao fault.

The 1964 Paiho earthquake shown as an asterisk in Figure 1 is the last damaged earthquake in this region. This earthquake caused hundreds of deaths and injuries. Chang and Yeh (1981) analyzed the teleseismic body waves to determine its focal mechanisms as strike: $\text{N } 2^{\circ}\text{E}$; dip: 48° ; and slip: 87° at the depth of 18 km. The results have been used as a strong evidence to explain the activity of the Chukou fault. However, there is no historical document giving evidence of surface faulting during the earthquake. With the hypocentral location of the 1964 Paiho earthquake adopted by Chang and Yeh (1981), it is about 5 km away from Chukou

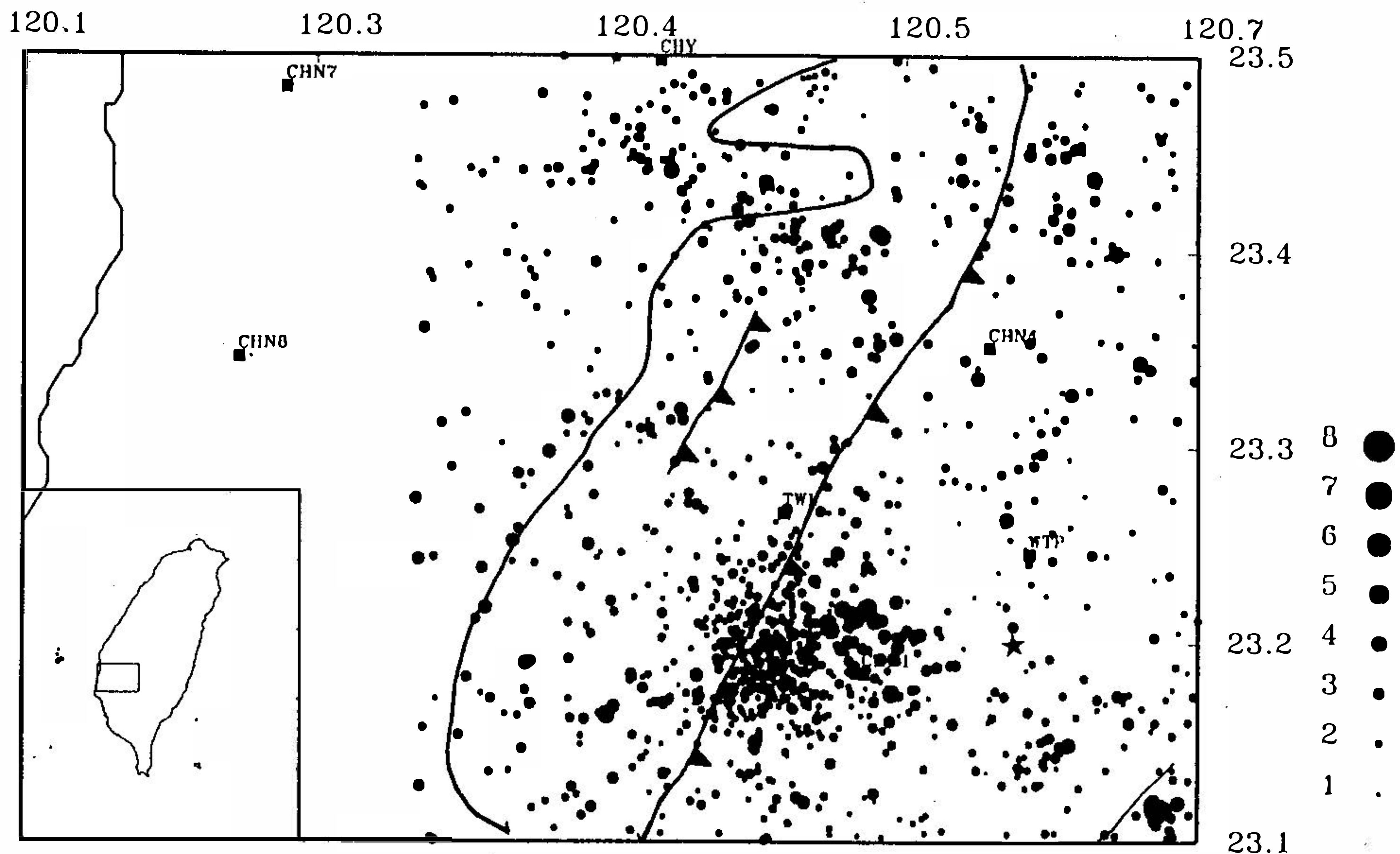


Fig. 1. Seismicity map of the Chia-Nan plain from 1991 to 30 June 1994. The stations shown belong to the TaiSeiN. The different types of lines indicate the geological boundary or fault. The detailed explanation is given in the text.

fault line observed on the surface. If a focal depth of 18 km is assumed, then the dipping angle of the fault plane must be greater than 75° . Otherwise, the Chukou fault would be more complicated faulting mechanisms than just a plane. All of these observations imply that the earthquakes occurring in this region is worthwhile to study in detail, and could be used as the supplemental interpretation for the Paiho earthquake.

3. DATA ANALYSIS

Six earthquakes of magnitudes greater than 3.5 which occurred during the period of the Tapu earthquake sequence are selected for moment tensor inversion. Table 1 lists the earthquake parameters determined by the TaiSeiN. The last column gives the number of strong motions used for waveform modeling of that earthquake and the instrument ID is listed below. Table 2 is the information about the strong motion stations used in this paper. The corresponding instrument ID installed at that station is in the second column. The initial "T" represents the instrument A900 (by Teledyne, 200 samples/second) and the "I" is the instrument IDS3600 (by Terra Tech., 250 samples/second). The number following the initial letter is the series number of the instrument. In order to distinguish the instrument type of the seismograms, the instrument ID is also used throughout the paper.

Based on two criteria, the digital strong motion data are selected to determine the focal mechanism by waveform modeling. The epicentral distance must be less than 20 km and the impulsive P- and S-waves ought to be able to be identified on the vertical and horizontal components respectively. The short epicentral distance is proposed because the seismic signal at short distance can provide information about the physics of the ruptural process without

Table 1. Hypocentral location of earthquakes.

Event	DATE	Origin Time (UT)	Location		Depth km	ML	NSM
			Latitude	Longitude			
1	15 Dec. 1993	21:49:43.21	23 12.80	120 31.22	13.50	5.70	3 I234,I229 T031
2	15 Dec. 1993	21:52:30.60	23 11.43	120 31.23	13.50	4.20	3 I234,I233 T031
3	15 Dec. 1993	22:01:36.66	23 12.39	120 33.10	12.60	3.71	2 I234,T031
4	20 Dec. 1993	03:32:03.36	23 13.10	120 30.73	16.00	4.41	3 I229,T031 T160
5	3 Jan. 1994	09:03:05.78	23 24.39	120 32.60	6.70	4.40	2 T018,I225
6	3 Jan. 1994	09:12:04.99	23 24.52	120 32.09	6.70	4.35	2 T018,T050

Table 2. Parameters of strong motion station.

Station Code	Instrument ID	Location	
		Latitude	Longitude
CHY010	I225	23 27.92	120 32.66
CHY014	I229	23 17.80	120 35.00
CHY018	I233	23 13.45	120 23.54
CHY019	I234	23 10.77	120 28.70
CHY042	T050	23 21.51	120 35.00
CHY057	T160	23 08.99	120 24.58
CHY062	T031	23 07.31	120 27.01
CHY087	T018	23 23.02	120 31.32

the contamination due to wave propagation. The P- and S-wavlets are the main parts of the seismogram used for moment tensor inversion. Additionally, the difference between the P- and S-wave arrivals is an important factor as considering the adjustment of epicentral distance since the hypocentral location determined by the TaiSeiN has been used. In practice, with the use of the TaiSeiN's hypocenter, it is required that the epicentral distance be slightly adjusted (less than 1.0 km) to fit the P- and S-wave arrivals especially for stations at short distance.

The acceleration seismograms are integrated once and twice to get velocity and displacement seismograms individually. A third-order bandpass butterworth filter with a frequency range from 0.4 Hz to 20.0 Hz are applied during the integration to remove the baseline drift. Figure 2 is an example of the data processing of the T031 recorded in event 2. The last three traces are displacement seismograms being rotated to become radial and tangential components from horizontal components (NS and EW) on the basis of the azimuth angle of the station to epicenter. These three displacement seismograms are actually used for waveform modeling. The numbers at the end of each trace are the peak values of each seismogram. When the onset amplitude of the P and S waves are compared, it is easy to find out that the amplitude of S wave is much larger than that of the P-waves, and the S-waves on the vertical

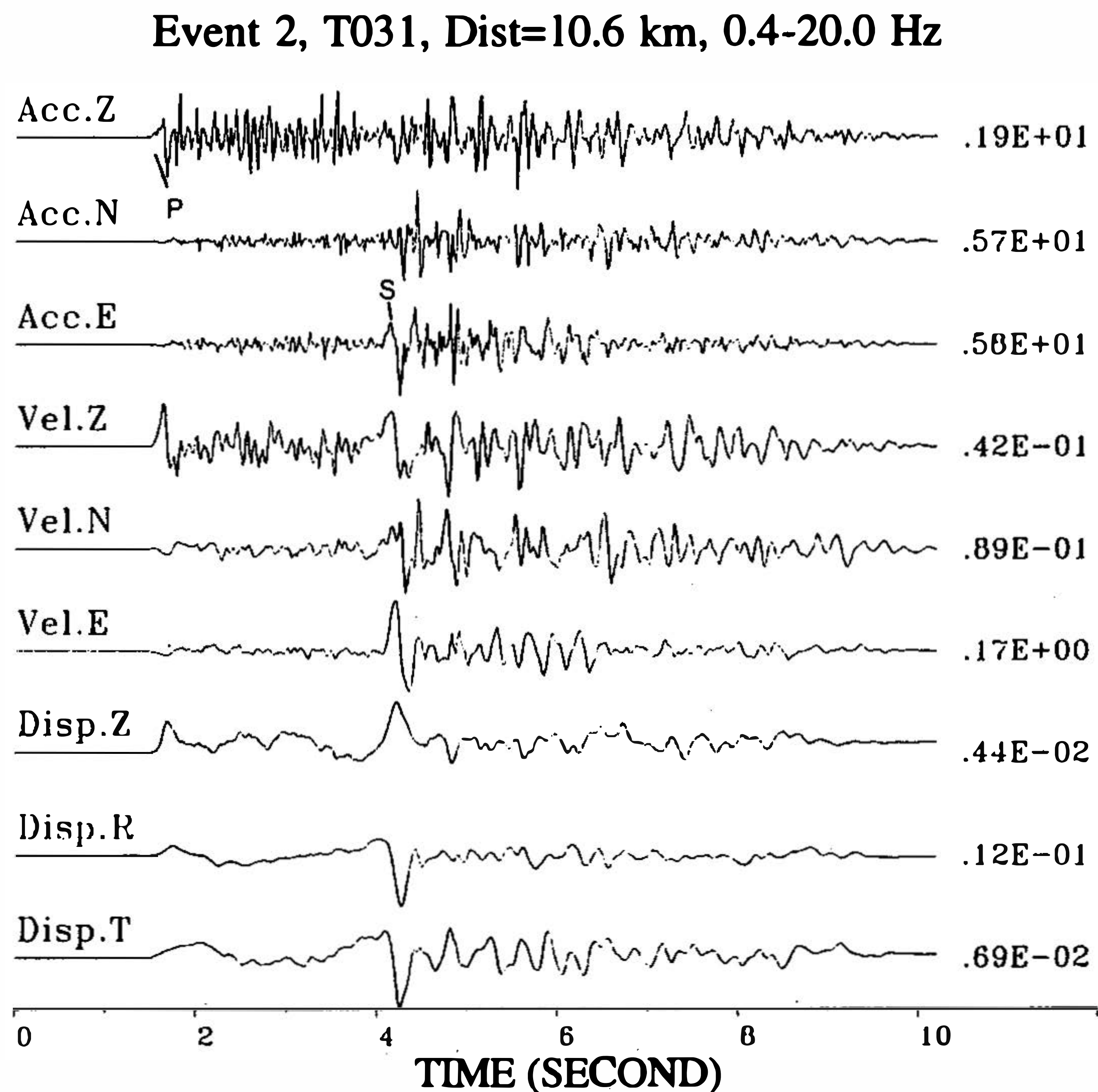


Fig. 2. Example of data processing. The first three traces are the original accelerograms. The integrated traces of velocity follow, while a third-order bandpass Butterworth filter in the frequency range of 0.4 Hz to 20.0 Hz is used to remove the baseline drift during integration. The last three traces are displacement seismograms which are used for moment tensor inversion.

component is implicit. These phenomena can also be found in most of the seismograms recorded in the Chia-Nan area no matter where the earthquake is. They can be explained as the effects of near surface sedimentation which causes the seismic wave incident vertically. Therefore, the S-wave is very clear on the horizontal components but barely noticeable on the vertical component. On the other hand, the P wave becomes the dominant phase on the vertical component but has a very small amplitude on the horizontal components.

4. RESULTS OF MOMENT TENSOR INVERSION

Table 3 presents the earth model used to generate the required Green's functions. The model is the layered model taken from Ho and Shin (1994), and it is only slightly modified at the top two layers according to the results of reflection seismics in the Chia-Nan area (Wang *et al.*, 1993; Shih *et al.*, 1993). The more realistic model is very important in the construction of synthetic seismograms especially for waveform modeling. It effects not only the amplitude fit but also the travel time fit of the P- and S-waves. All Green's functions were calculated using only the far-field asymptotic terms since only high-frequency signals were of interest, and the direct (P- and S-) and surface converted rays were calculated. In order to have the same frequency range, the Green's functions were identically filtered as observed data.

Table 3. Earth model.

P Velocity (km/Sec)	S Velocity (km/Sec)	Density (gm/cm)	Thickness (km)
2.50	1.40	1.65	0.20
3.50	2.00	2.00	0.80
3.78	2.20	2.20	3.00
5.04	3.03	2.31	5.00
5.71	3.26	2.40	4.00
6.03	3.47	2.51	4.00
6.44	3.72	2.63	8.00
6.83	3.99	2.70	5.00
7.28	4.21	3.30	-

The direct P, SV and SH are the main ray paths for synthetic calculation and waveform inversions while the conversion waves of P to S were also considered in the final waveform matching. The hypocentral information listed in Table 1 was used to calculate Green's functions. ~~In order to have good fitting of the P- and S- wave arrivals, the epicentral distance~~ from the station is allowed to be adjusted by no more than 1 km. The source time function was approximated by using a parabolic-shaped pulse with a duration width of 0.3 seconds for event 1 and 0.2 seconds for the others. The green's functions were identically filtered as observed data. The elastic attenuation was negligible since the short distance seismograms were used, and the effects are not significant especially as the multiple station moment tensor is applied while they share the same attenuation effects.

Following Jost and Herrmann (1989), the symmetric moment tensor is represented in terms of M11, M12, M13, M22, and M23. These five elements can be inverted directly from a least-square sense. The cut-off eigen value inversion scheme is applied as the matrix is inverted. The threshold value is set at 10^{-5} of the largest eigen value. The inversion procedure is similar to that of Jost and Herrmann (1989) and Huang (1994). Instead of using only the peak amplitude of the SH wave (Jost and Herrmann, 1989) and full waveform (Huang, 1994), the direct P- and S- wavelets of about 1 second window length are used. This method can include as much information in waveform and reduce errors in inversion caused by the unknown waveforms between P- and S-wave arrivals. Considering the small amplitudes of the P-waves compared to those of the S- waves due to the effects of near surface sedimentation, a multiple station moment tensor inversion is used because single station inversion always indicates that the station's located close to the nodal planes of the focal mechanism (Figure 3). As seen from the figure, both of observed and synthetic seismograms are dotted in pair. The synthetic seismograms are calculated using the fault plane solutions plotted on the right hand side which are the results of moment tensor inversion. The good fit in waveform modeling does not mean that the solutions have physical meanings in some extreme cases. Actually, this result is to be expected and is discussed later.

The multiple station inversion results are summarized in Table 4. The moment tensor element can be decomposed into double couple focal mechanisms and Compensated Linear Vector Dipole (CLVD) components. The smaller contribution of the CLVD component in Table 4 indicates that the ruptural processes of all earthquakes are characterized primarily by a major double couple mechanism. The seismic moment is calculated by the diagonalized matrix of moment tensor. The value of $0.494e+24$ dyne-cm of the mainshock is consistent with the results obtained by using the Lg-wave spectral analysis (Chiang and Shin, 1994)

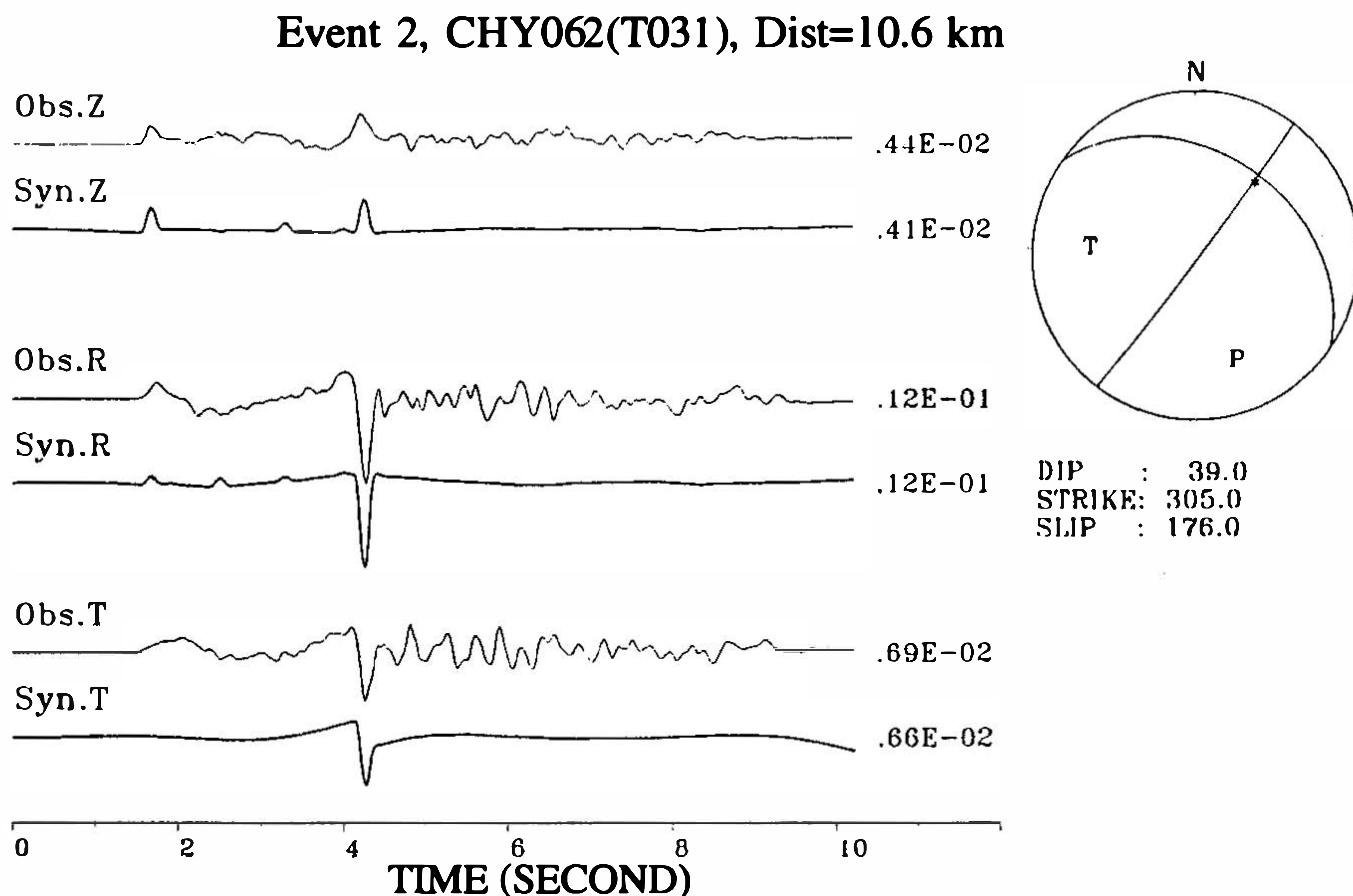


Fig. 3. Results of the single station moment tensor inversion. The waveforms are fairly well matched. All traces are filtered in the frequency range of 0.4 Hz to 20.0 Hz. The comparison of the observed and inverted synthetic waveforms are on the left, while the corresponding fault plane solutions are plotted on the right. The asterisk in the fault plane solution plot represents the location of the station projected on the low hemisphere. Its closing to the nodal plane is due to the sedimentary site effects.

for the mainshock of the Tapu earthquake sequence. Figure 4 is the waveform matching of the observed and inverted synthetic seismograms for these 6 earthquakes. The inverted fault plane solutions are plotted on the right. For each event, only one station waveform matching is demonstrated. The asterisk represents the location of the station on the low hemisphere projection, while the circles represent the other stations used in the same multiple station moment tensor inversion. The traces in Figure 4 are all normalized by a proper factor to make the comparison more visual. The peak amplitude in centimeter units appears at the end of each trace. When Figures 4b and 2 are compared, the importance of multiple station moment tensor inversion especially for seismograms recorded at the sedimentational site is evident. The waveform matching from single station inversion is as good as those from multiple station moment tensor inversion. However, the fault plane solutions are totally different. Undoubtedly, the solutions from multiple station moment tensor are much more reliable because of more constraints involved.

The results of moment tensor inversion for the 6 earthquakes indicate that the Tapu earthquake and its aftershocks (events 2, 3 and 4) are dominant thrust focal mechanisms of fault plane solutions: dip= 50° - 60° ; strike= 170° - 200° ; and slip= 60° - 80° . They are similar to the results from the first motion analysis obtained using the short-period seismograms of the TaiSeiN (Chang and Shin, 1994). For events 5 and 6, they show an almost vertical dipping plane of a normal faulting with a left-lateral component. The reasons for choosing these fault plane solutions as faulting planes as listed in Table 4 are explained in the next section.

Table 4. Summary results of moment tensor inversion.

	Event 1	Event 2	Event 3	Event 4	Event 5	Event 6
MOMENT TENSOR ELEMENT						
(dyne-cm)						
M11	-.75989E+23	-.35071E+21	-.85807E+21	-.27624E+22	.50207E+21	.49807E+21
M12	-.30726E+24	-.84477E+21	-.44539E+21	-.20317E+21	-.37642E+22	-.39943E+22
M13	.45231E+22	-.24505E+21	.57873E+20	-.63408E+20	.44001E+22	.47211E+22
M22	.46016E+24	.17818E+22	.17609E+22	.51579E+22	-.66367E+21	-.75987E+21
M23	-.40563E+23	-.96923E+21	-.83255E+21	-.29991E+22	.11865E+22	.16911E+22
SEISMIC MOMENT						
(dyne-cm)						
	.49401E+24	.20637E+22	.16143E+22	.48359E+22	.55210E+22	.60168E+22
DOUBLE-COUPLE						
DIP	48.0°	62.0°	63.0°	65.0°	88.0°	86.0°
STRIKE	200.0°	178.0°	175.0°	173.0°	106.0°	112.0°
SLIP	84.0°	64.0°	70.0°	79.0°	-118.0°	-113.0°
% OF CLVD	3.0	1.0	3.0	3.0	2.0	3.0

5. DISCUSSIONS AND CONCLUSIONS

In this paper, the digital strong motion seismograms recorded during the 1993 Tapu earthquake sequences are used for inversion of the moment tensor of the source rupture. The multiple station moment tensor inversion scheme is applied to reduce bias in the solutions due to the sedimentational site effects in the Chia-Nan area. From the decomposition of the moment tensor, the smaller contribution of the CLVD component of all earthquakes indicates that the source ruptures are dominantly characterized as a double couple focal mechanism. The fault plane solutions can be divided into two different groups. The Tapu earthquake and its aftershocks (events 2, 3 and 4) are in the same group of dominant thrust faulting. On the other hand, the second group including event 4 and 5 reveal an almost vertical normal faulting. The epicenters of the earthquakes in the second group are located at about 20 km north of the first (Figure 5). The difference in locations and focal mechanisms might imply that they are two separate earthquake sequences occurring within a short time period.

Figure 5 is the seismicity map of earthquakes in the Chia-Nan area from 15, December 1993 to 30, January 1994. The numbers indicate the earthquakes used for moment tensor inversion. As can be seen, two concentrated clusters in a mostly east-west trend can be found. The south cluster actually belongs to the 1993 Tapu earthquake sequence. The north cluster began on 3 January 1994, while the Tapu earthquake sequence was still occurring. The depth cross section of the Tapu earthquake sequence along AA' (approximately perpendicular to the Chukou fault) is shown in Figure 5b. The dipping western trend is clear. It is also one of the fault planes obtained from the moment tensor inversion and the one listed in Table 4. Figure 5c is the depth cross-section of earthquakes for the north cluster along BB'. Although the distribution of the earthquakes is concentrated shallowly from 3 km to 10 km., a steep linear trend agrees with the fault plane solutions obtained from the moment tensor inversion.

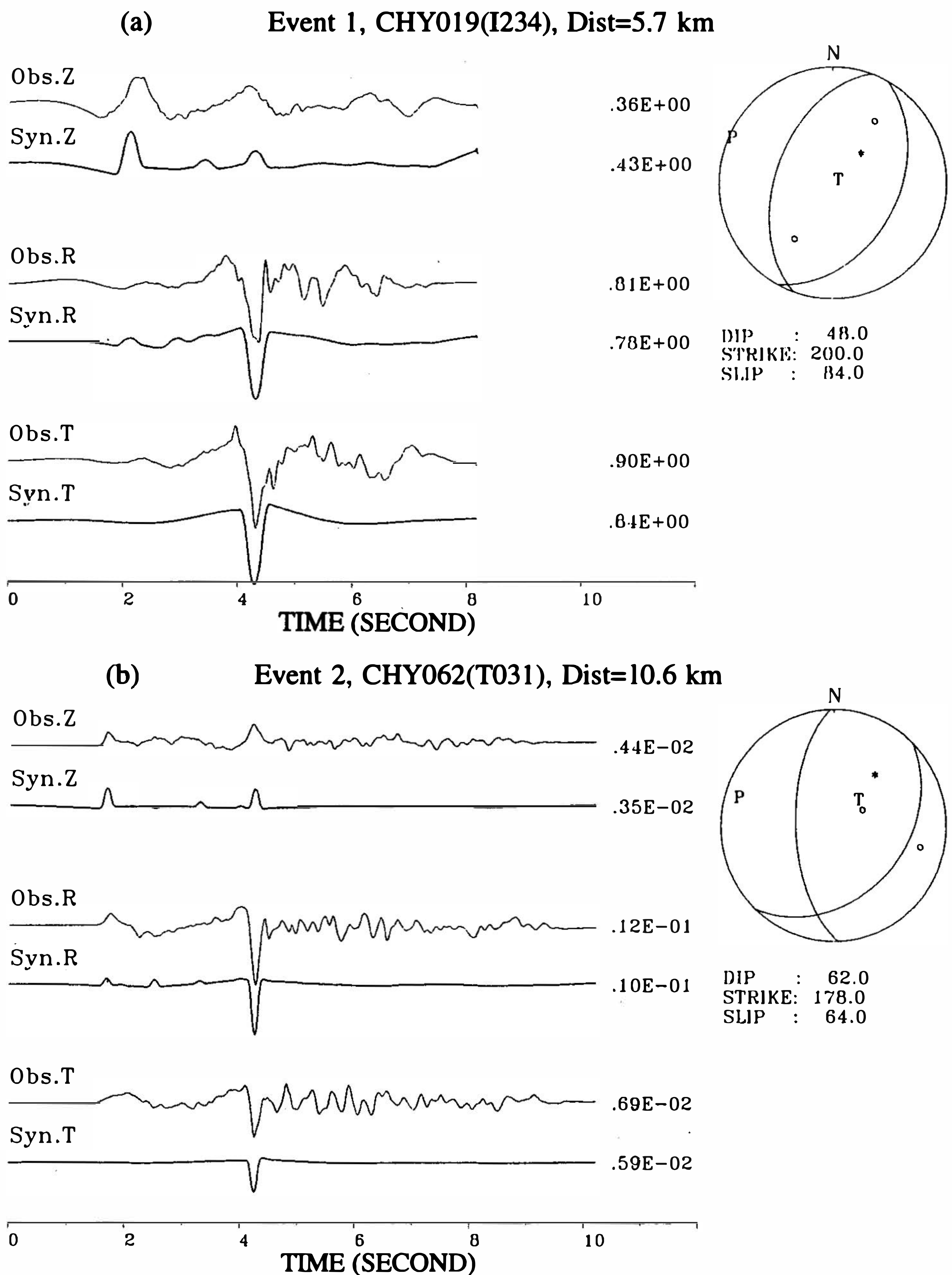


Fig. 4. Results of multiple station moment tensor inversion and waveform modeling for 6 earthquakes. The same notations are used as in Figure 3. The circles on the fault plane projection sphere indicate the location of the other stations used in the same moment tensor inversion. (a) Event 1, mainshock of the Tapu earthquake sequence. (b) Event 2 which is the same event as in Figure 3. The difference between a single-station and a multiple-station moment tensor inversion can be easily identified in this comparison. (c), (d), (e), and (f) are for events 3, 4, 5 and 6, respectively.

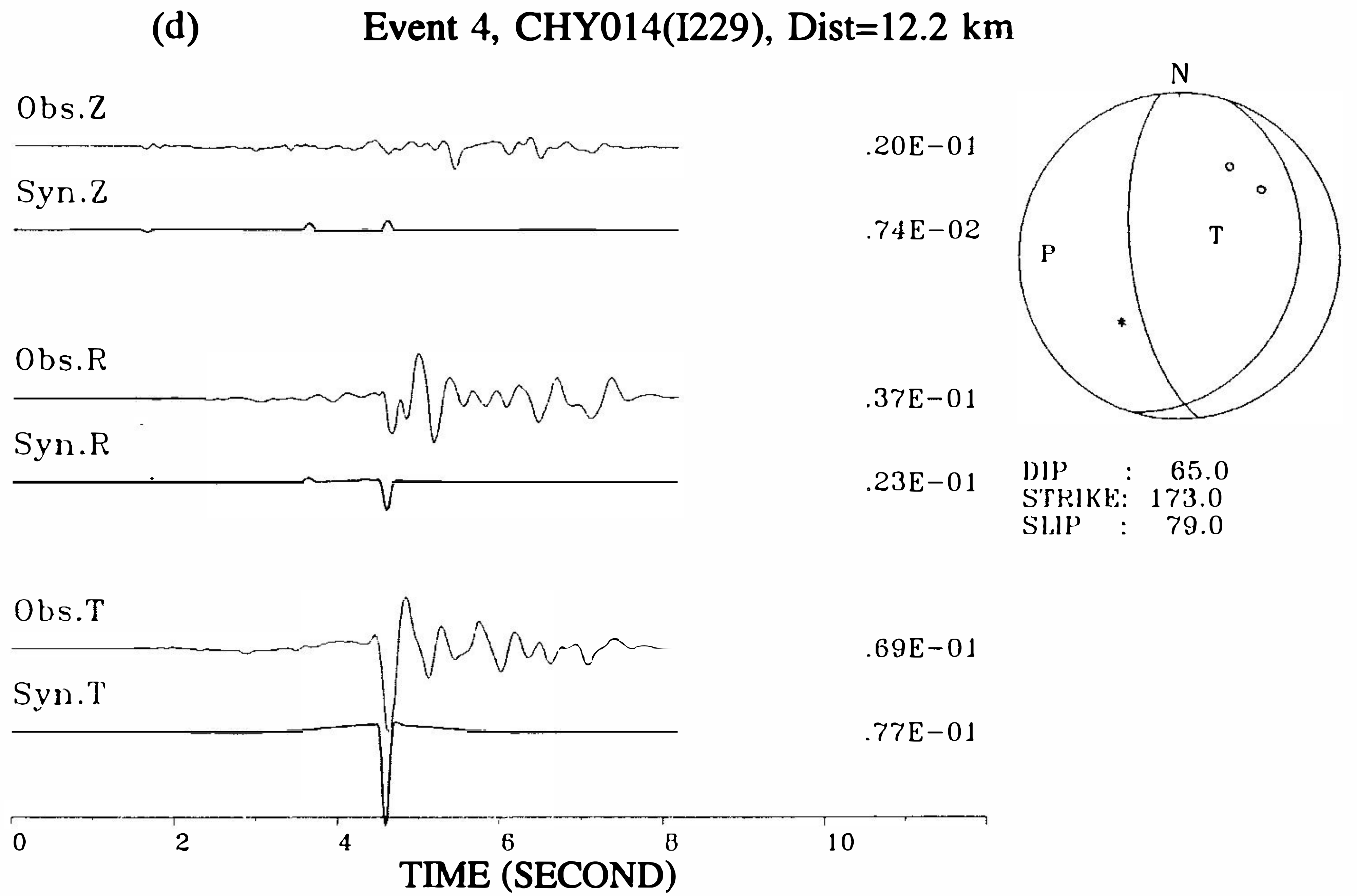
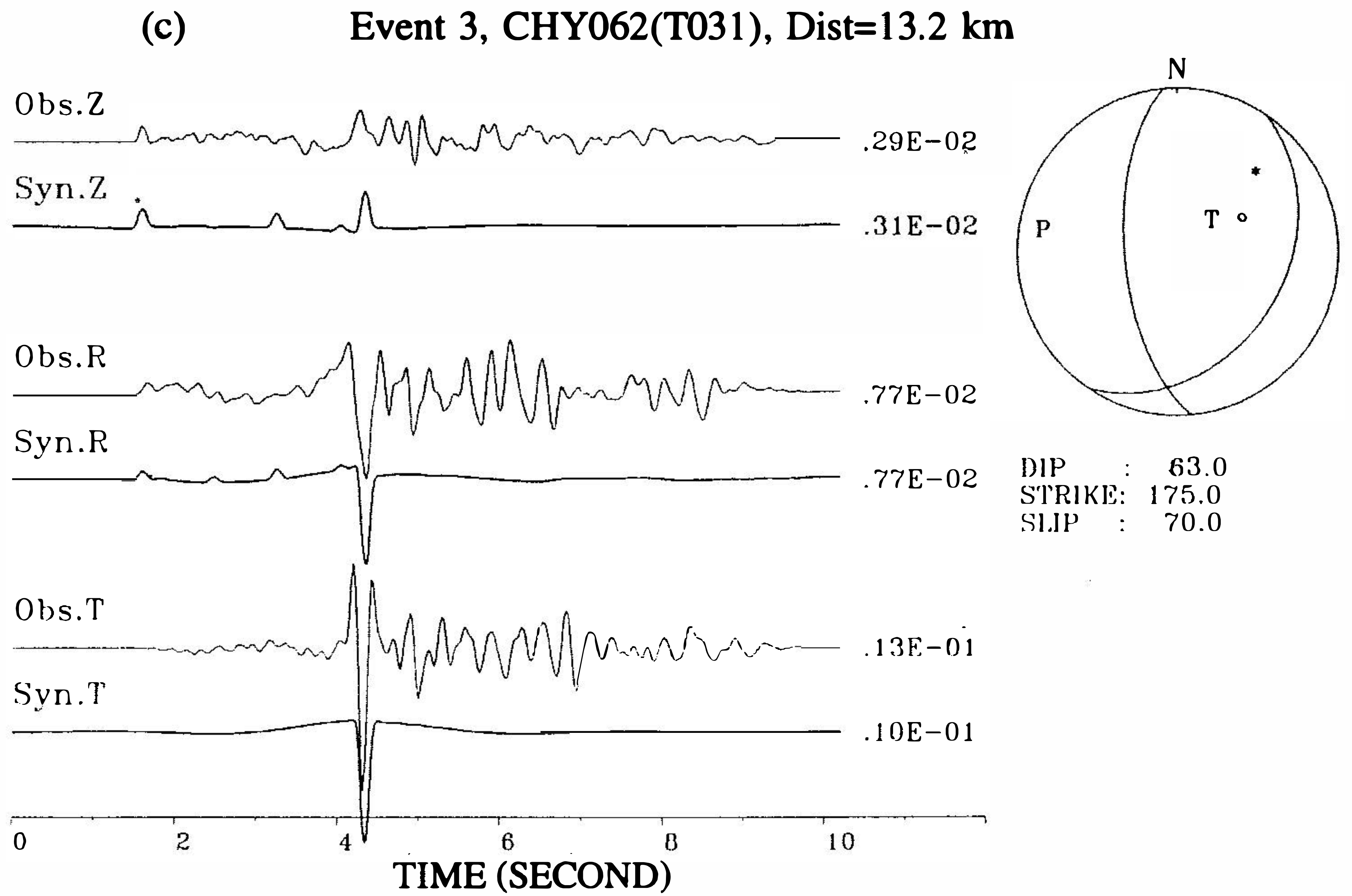
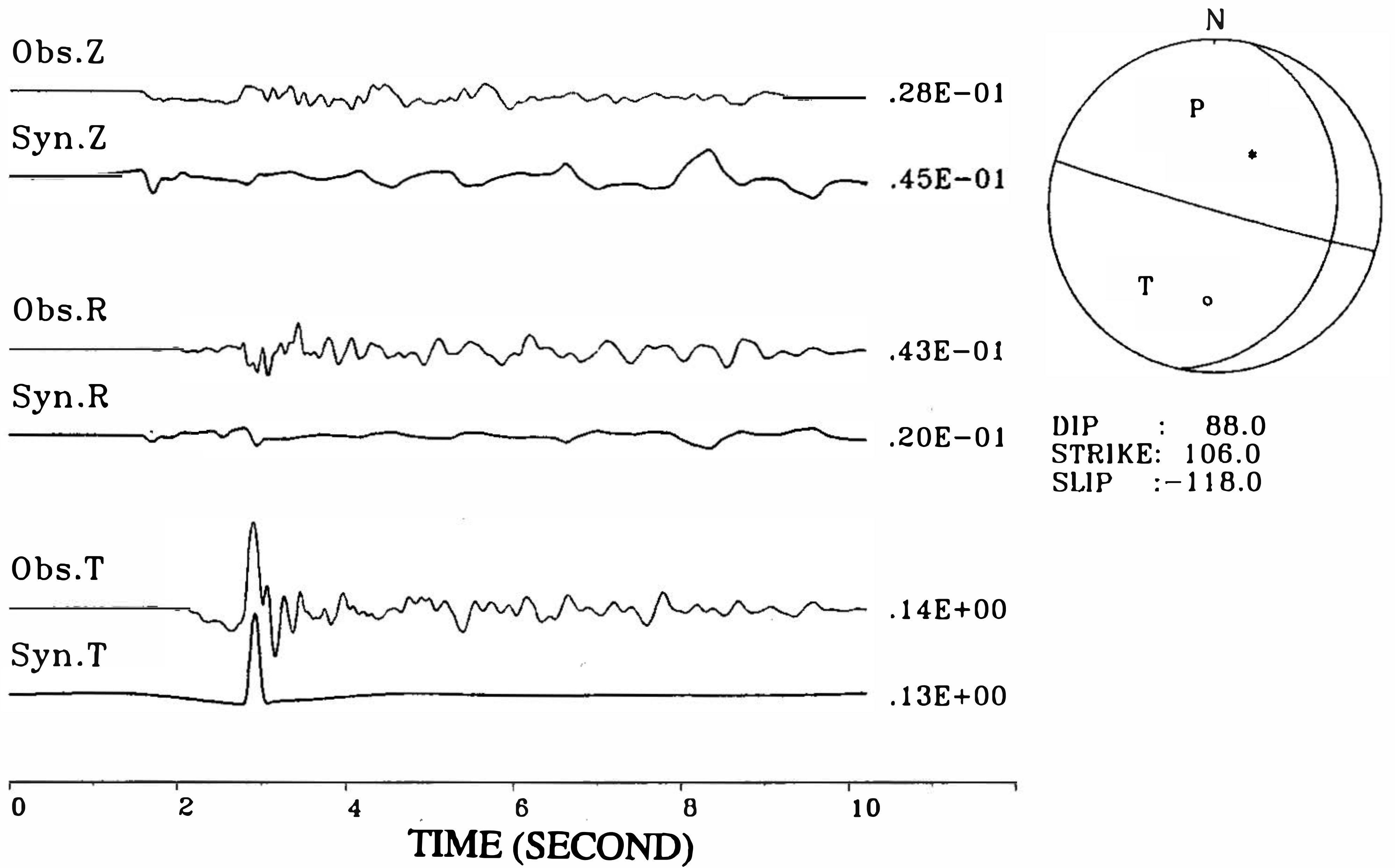


Fig. 4. (Continued)

(e) Event 5, CHY087(T018), Dist=3.0 km



(f) Event 6, CHY042(T050), Dist=7.5 km

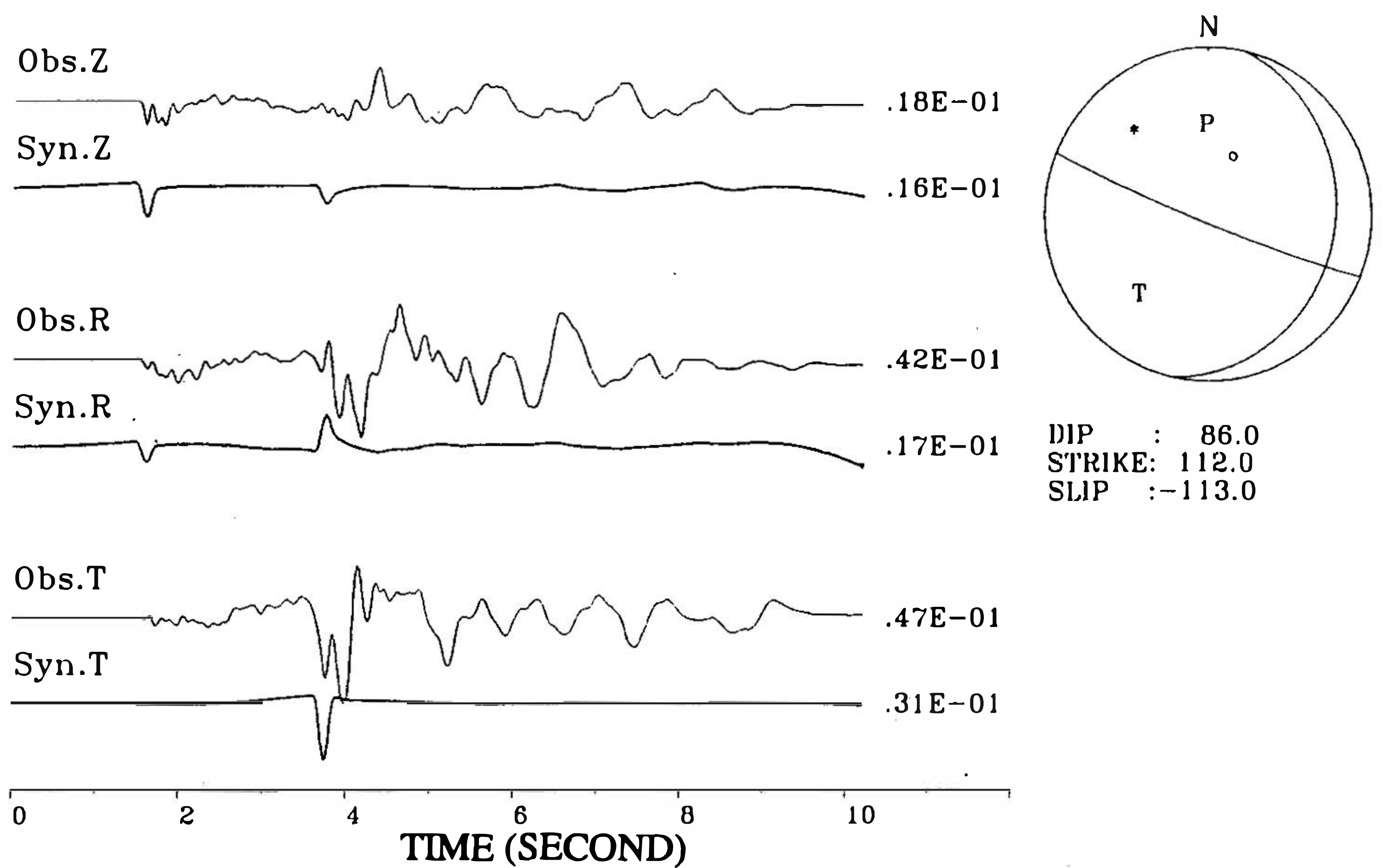
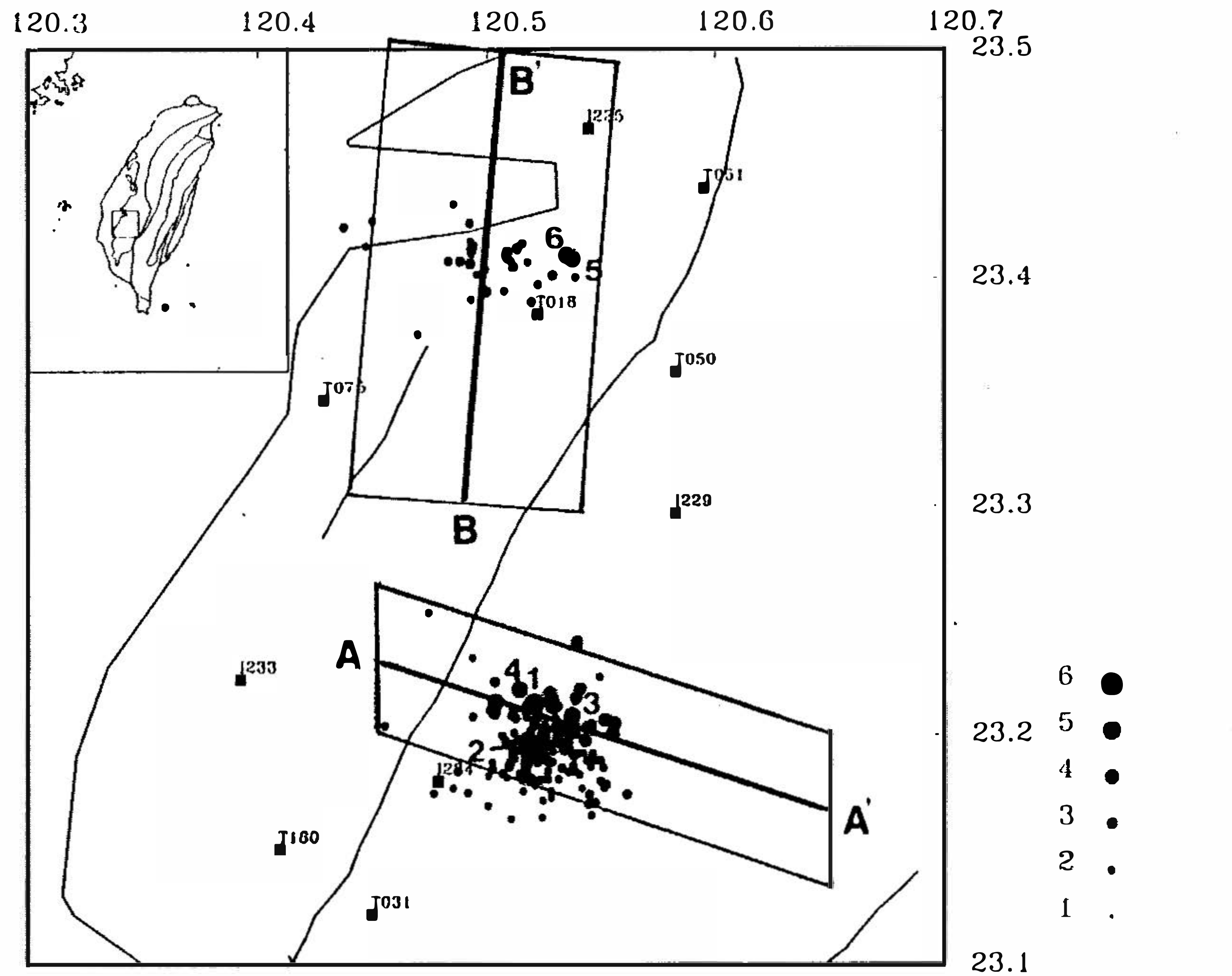
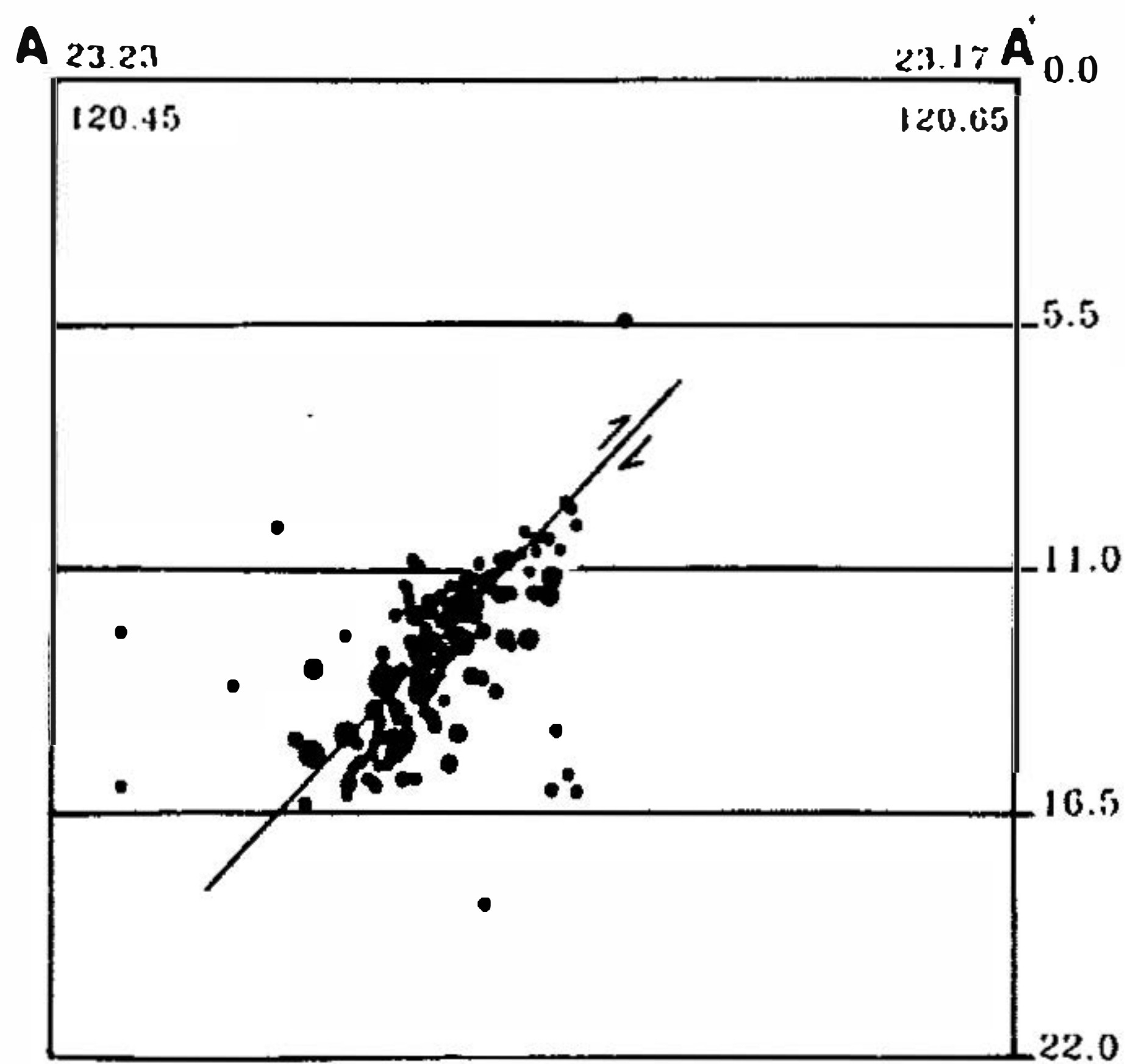


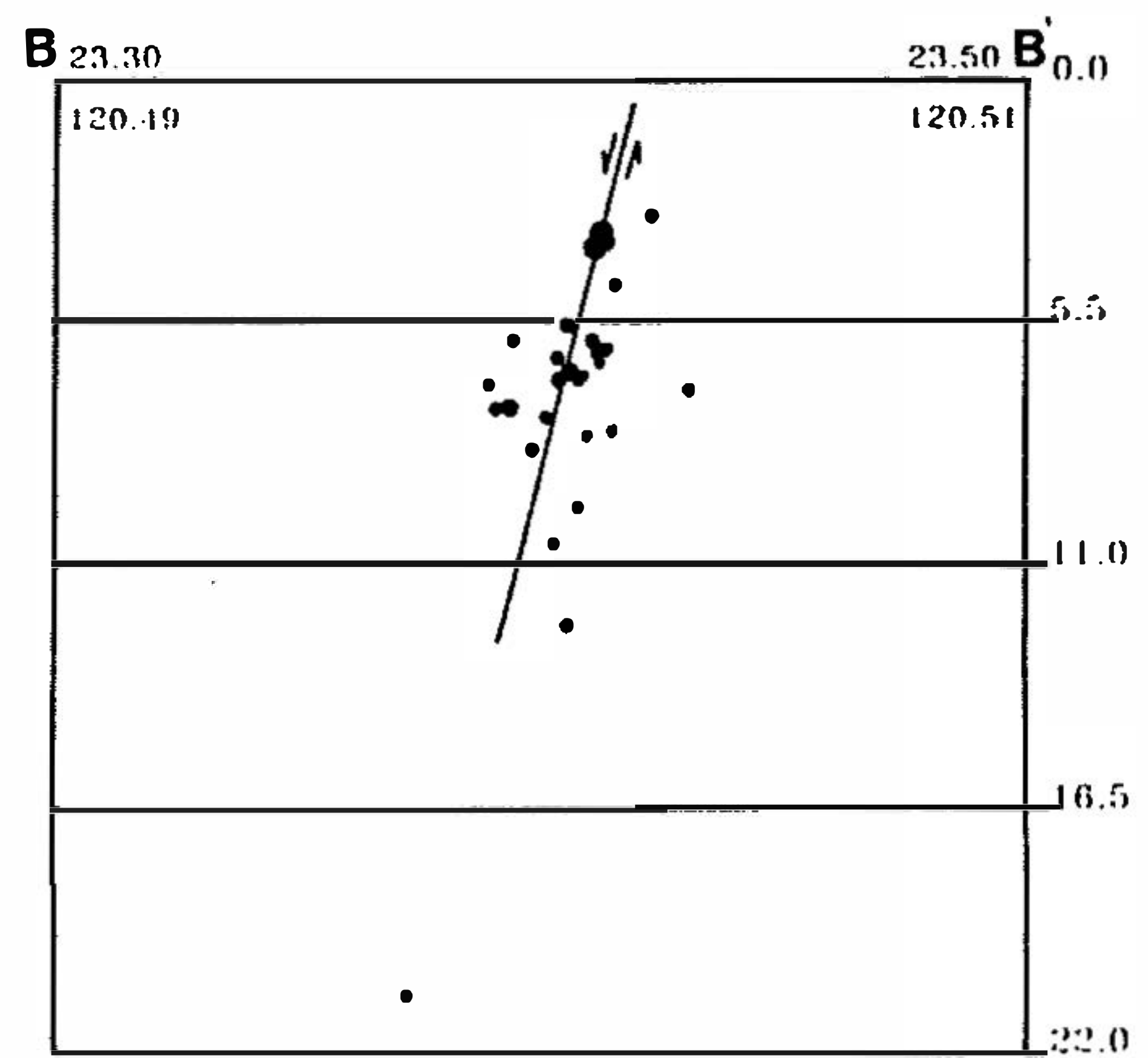
Fig. 4. (Continued)



(a)



(b)



(c)

Fig. 5. Seismicity map and cross-sections for earthquakes which occurred from 15, December 1993 to 30, January 1994. (a) The earthquake distribution map. Two concentrated clusters are found. (b) The cross-section of the hypocenters along AA'. The fault plane based on the moment tensor inversion is also shown. (c) The cross-section of the hypocenter along BB'. The line with the relative displacement arrow indicates the fault plane obtained in this paper.

With the results of the moment tensor inversion and the analysis of the depth cross-sections of earthquakes combined, it appears that two earthquake sequences occurred in about 40 days. The Tapu earthquake sequence has ruptural mechanisms with NNE thrust faulting in westward dipping. Chang and Yeh (1981) analyzed the 1964 Paiho earthquake and adopted the eastward dipping plane as the faulting plane to fit the geological mapping and faulting system in the vicinity. But, the auxiliary plane is identical to the plane chosen in this paper. The close hypocentral locations of the Tapu and Paiho earthquakes and the dipping angle of the faulting plane obtained from both studies imply that these two earthquakes were essentially caused by the same faulting plane, which is not directly related to the Chukou fault. The second earthquake sequence started on 3, January 1994 with a mainshock magnitude of 4.4. The hypocentral locations were at about 20 Km north of the Tapu earthquake. The vertical normal faulting with a left-lateral component is adequate to explain the ruptural mechanisms of this earthquake sequence.

In the past 3 years, several earthquake sequences have occurred in the Chia-Nan area, such as the 1991 Chiali earthquake sequence (Shin *et al.*, 1994) and the 1993 Tapu earthquakes sequence in this paper. All the results of a detailed investigation show that the occurrence of these earthquake sequences are not associated with the geological structure and faulting system in the area. On the contrary, they imply that the local stress and complicated geological environment play very important roles especially when a seismic hazard analysis of the Chia-Nan area is under consideration.

REFERENCES

- Chang L. S., and Y. T. Yeh, 1981, A source model of the Paiho, Taiwan earthquake from the inversion of teleseismic body waveforms, National Science Council Rep., Taiwan, 65pp.
- Chang, C. H., and T. C. Shin 1994: Earthquakes in 1993. Accepted by Meteor. Bull.
- Chiang, C. H., and T. C. Shin, 1994: Source scaling model in the Taiwan area. *Meteor. Bull.*, **40**, 235-245.
- Ho, M. Y., and T. C. Shin, 1994: Three dimensional velocity structure of western Taiwan. *Meteor. Bull.*, **40**, 216-234.
- Ho, C. S., 1988: An introduction to the geology of the Taiwan explanatory text of the geologic map of Taiwan. Central Geological Survey, Taiwan, 192pp.
- Hsu, T. L., and H. C. Chang, 1979: Quaternary faulting in Taiwan. *Mem. Geol. Soc. China.*, **3**, 155-165.
- Huang, B. S., 1994: Estimation of source parameters by the inversion of near source strong motion wave forms. *TAO*, **5**, 11-26.
- Jost, M. L., and R. B. Herrmann, 1989: A student's guide and review of moment tensors. *Seism. Res. Lett.*, **60**, 36-57.
- Shin T. C., and P. L. Leu, 1986: Study on the earthquake potential in the Taiwan area. *Meteor. Bull.*, **36**, 129-136.
- Shin, T. C., C. H. Chang, and C. H. Chiang, 1994: The March 1991 Chiali earthquake sequence. *Meteor. Bull.*, **40**, 17-36.

